

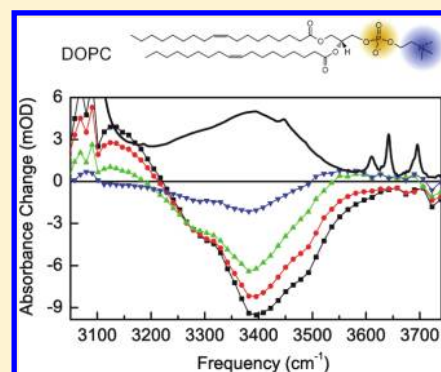
# Ultrafast Vibrational Dynamics of Water Confined in Phospholipid Reverse Micelles

Rene Costard,<sup>\*,†</sup> Nancy E. Levinger,<sup>‡</sup> Erik T. J. Nibbering,<sup>†</sup> and Thomas Elsaesser<sup>\*,†</sup>

<sup>†</sup>Max-Born-Institut für Nichtlineare Optik und Kurzzeitspektroskopie, Max-Born-Str. 2 A, D-12489 Berlin, Germany

<sup>‡</sup>Department of Chemistry, Colorado State University, Fort Collins, Colorado 80523-1872, United States

**ABSTRACT:** Ultrafast dynamics of OH stretching excitations of H<sub>2</sub>O confined in dioleoylphosphatidylcholine (DOPC) reverse micelles, a phospholipid model system, are studied in femtosecond pump–probe experiments. Measurements in a wide range of hydration show that spectral diffusion within the OH stretching band accelerates substantially with increasing water content. Concomitantly, the OH stretching lifetime decreases from approximately 500 fs at a 1:1 ratio of water and DOPC molecules ( $w_0 = 1$ ) to 300 fs for large water pools (ratio 16:1,  $w_0 = 16$ ). Two-color pump–probe studies mapping the ultrafast OH bending response after OH stretch excitation demonstrate that the relaxation pathway of the OH stretch vibration involves the OH bending mode. After OH stretch relaxation at high hydration levels, vibrational excess energy is randomized within the water pool and then transferred to the surrounding solvent.



## INTRODUCTION

The presence of water layers and water shells is essential for the structural and functional properties of biomolecular systems.<sup>1,2</sup> In most cases, biomolecules offer a large number of highly heterogeneous hydration sites at which water molecules interact with specific functional groups. Both local hydrogen bonding and—in dipolar or ionic systems such as phospholipid membranes or DNA oligomers—long-range Coulombic interactions are relevant, resulting in hydrogen bond geometries, interaction strengths, and orientational dynamics of water molecules significantly different from those of the bulk liquid. At physiological temperatures, water shells display pronounced structural fluctuations with elementary molecular motions and processes in the femtosecond time domain.

In recent years, ultrafast vibrational spectroscopy has provided specific insight into structural fluctuations of aqueous systems and into the underlying molecular interactions. Such work has mainly focused on neat water (H<sub>2</sub>O), isotopically diluted water (HOD in H<sub>2</sub>O or D<sub>2</sub>O), and other hydrogen-bonded liquids (for a review, see refs 3 and 4). Hydrated biomolecular systems such as phospholipid membranes and/or DNA have been studied to a much lesser extent, mainly because of their structural complexity and the resulting highly congested vibrational spectra.<sup>5–8</sup> As a result, there has been a quest for structurally simpler artificial model systems which allow for studying hydration processes under well-defined conditions and in a wide hydration range. The most prominent among such systems are reverse micelles containing a confined pool of water and separating it from a nonpolar liquid environment.<sup>9</sup>

Reverse micelles are formed in nonpolar solvents when surfactant molecules self-assemble into spherical particles, with the hydrophilic heads pointing to the inside.<sup>10</sup> In this way, variable amounts of water can be dissolved and confined in the

interior of the reverse micelles. Usually, the water content is characterized by the parameter  $w_0 = [\text{H}_2\text{O}]/[\text{surfactant molecules}]$  where the square brackets indicate the concentration of the respective species. Recently, we introduced dioleoylphosphatidylcholine (DOPC, upper part of Figure 1) self-assembled into phospholipid reverse micelles as a new model system to investigate the properties and function of water bound to biological membranes.<sup>11</sup> In a first series of experiments, we studied phosphate–water interactions by mapping the ultrafast response of the antisymmetric PO<sub>2</sub><sup>−</sup> stretching vibration. We found that the presence of a water pool accelerates the randomization of vibrational excess energy substantially by serving as an efficient heat sink. Here, we investigate the dynamics of water inside DOPC reverse micelles to gain a deeper understanding of water–phospholipid interactions.

Numerous studies have focused on discerning the dynamics of water molecules which interact with the hydrophilic head groups from water molecules in the more bulklike inner volume of the reverse micelles.<sup>12</sup> Detailed experimental work based on femtosecond infrared pump–probe and two-dimensional spectroscopy has been reported for dioctyl sodium sulfosuccinate (AOT) reverse micelles filled with isotopically diluted water (HOD in H<sub>2</sub>O or D<sub>2</sub>O)<sup>13–15</sup> or with neat water (H<sub>2</sub>O).<sup>16–18</sup> In the HOD systems, highly diluted OD or OH stretch oscillators probe ultrafast changes of liquid structure which lead to spectral diffusion, anisotropy decays, and other changes of the vibrational excitations. In neat water, both the coupling between the two OH oscillators of the H<sub>2</sub>O molecule and resonant energy transfer between water molecules

Received: April 23, 2012

Published: April 30, 2012

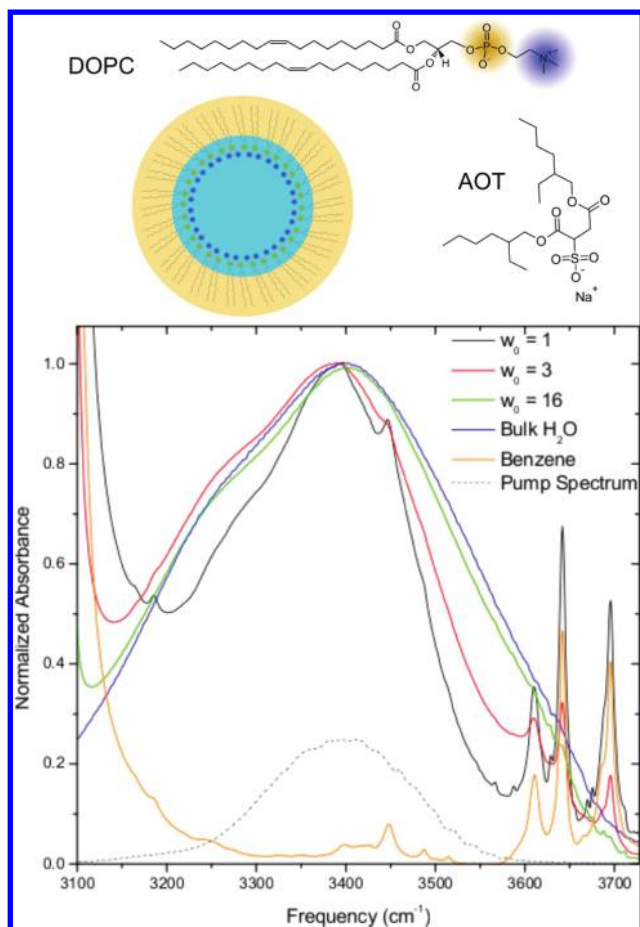


**Figure 1.** Upper part: molecular structures of DOPC and AOT and schematic of a micelle structure. Lower part: normalized infrared absorption spectra of DOPC reverse micelles dissolved in benzene for different values of  $w_0$ . The absorption spectra of bulk H<sub>2</sub>O and neat benzene are also shown. Dashed line: spectrum of femtosecond pump pulse centered at 3400 cm<sup>-1</sup>.

contribute to vibrational dynamics, on top of structural dynamics of the water pool. Data for both types of systems have been interpreted in terms of a so-called core-shell model to distinguish two water species dynamically. Recent theoretical and experimental work has, however, revealed limitations of this picture.<sup>14,19</sup> Energy transport from a reverse micelle's water pool that was heated via the decay of OH stretch excitations to the environment has been studied in some detail, and heat diffusion models have been invoked to account for the pico- to nanosecond kinetics.<sup>20,21</sup> However, the pathway of OH stretch relaxation has remained controversial. For bulk water a predominant decay via the OH bending mode was observed.<sup>22</sup> In contrast, several studies of water shells in AOT reverse micelles<sup>16,18</sup> and water bound to phospholipid bilayers<sup>23</sup> propose a relaxation into low-frequency hydrogen bond and solvent modes.

The molecular structure of DOPC (upper part of Figure 1) is markedly different from AOT which contains an anionic sulfonate headgroup SO<sub>3</sub><sup>-</sup> with sodium counterions. DOPC and phospholipids display a zwitterionic structure with a PO<sub>4</sub><sup>-</sup> unit and a covalently linked counterionic, e.g., choline group. The hydration of the choline group derived from neutron diffraction experiments<sup>24</sup> differs significantly from hydration of

free sodium cations<sup>25</sup> or sodium cations associated with counteranions.<sup>26</sup>

In this article, we address the dynamics of H<sub>2</sub>O in DOPC reverse micelles. This system is chosen because of its relevance for phospholipid systems in their native H<sub>2</sub>O environment. The ultrafast dynamics of OH stretching excitations is studied in femtosecond pump-probe experiments. The line shape of the OH stretching band undergoes a pronounced reshaping which occurs on a time scale of 1–2 ps at  $w_0 = 1$  and accelerates with increasing water concentration. The OH stretch lifetime displays a decrease from approximately 500 fs at  $w_0 = 1$  to 300 fs at  $w_0 = 16$ . Two-color pump-probe studies clearly demonstrate that the OH stretch relaxation pathway involves the OH bending mode.

## EXPERIMENTAL TECHNIQUES

The sample preparation and the femtosecond pump-probe setup have been described in detail elsewhere.<sup>11</sup> Briefly, a 0.25 M solution of DOPC (Avanti Polar Lipids) in benzene (Sigma-Aldrich, anhydrous 99.8%) was prepared, and appropriate amounts of water were added to obtain samples with  $w_0 = 1, 3$ , and 16. For steady-state and time-resolved measurements, these samples were held between two 1 mm thick CaF<sub>2</sub> windows with respective sample thicknesses of 100, 25, and 6 μm to obtain optical densities in the OH stretch absorption range of <0.6.

Independently tunable mid-infrared pump and probe pulses were generated with home-built optical parametric frequency converters<sup>27</sup> pumped by a commercial regeneratively amplified Ti:sapphire laser (center wavelength 800 nm, repetition rate 1 kHz). Pump pulse energies were <2 μJ, and the spectral bandwidth of the pump pulses was 175 cm<sup>-1</sup> (fwhm). The cross-correlation width of pump and probe pulses was <150 fs. After interaction with the sample, the probe beam was dispersed in a monochromator, detected by a 64-pixel MCT detector array, and the pump-induced absorbance changes  $\Delta A = -\log(T/T_0)$  (where  $T$  and  $T_0$  are the sample transmissions with and without excitation) were measured as a function of the pump-probe delay time. Measurements with parallel and perpendicular linear polarizations of pump and probe pulses and under magic-angle polarization ( $\theta = 54.7^\circ$ ) were performed by rotating the probe polarization by 45° with respect to the pump and using a polarizer after the sample interaction to choose the respective polarizations. In selected measurements, the pump-probe anisotropy  $r(t)$  is constructed by evaluating  $r(t) = [\Delta A_{||} - \Delta A_{\perp}] / [\Delta A_{||} + 2\Delta A_{\perp}]$ , where  $[\Delta A_{||} + 2\Delta A_{\perp}]$  is a rotation-free (so-called isotropic) signal and  $\Delta A_{||}$  and  $\Delta A_{\perp}$  are the absorption changes measured with parallel and perpendicular polarizations of pump and probe pulses.

## RESULTS

**Linear Vibrational Absorption Spectra.** Figure 1 shows the DOPC molecular structure as well as the normalized OH stretching absorption bands of water for different water concentrations  $w_0$  and of bulk water. The narrow absorption bands at 3450 cm<sup>-1</sup> and above 3600 cm<sup>-1</sup> are caused by the solvent benzene as is evident from a comparison with the absorption spectrum of neat benzene (orange line). With increasing hydration ( $w_0$ ), the spectral width of the OH stretching band increases, whereas the spectral position of the maximum of OH stretch absorption band remains nearly unchanged. Such behavior is different from AOT reverse

micelles where pronounced changes of line shape and spectral position of the OH stretching band occur with increasing  $w_0$ .<sup>18</sup>

#### Time-Resolved Pump–Probe Data. Transient Spectra.

Figure 2 shows transient spectra after OH stretch excitation

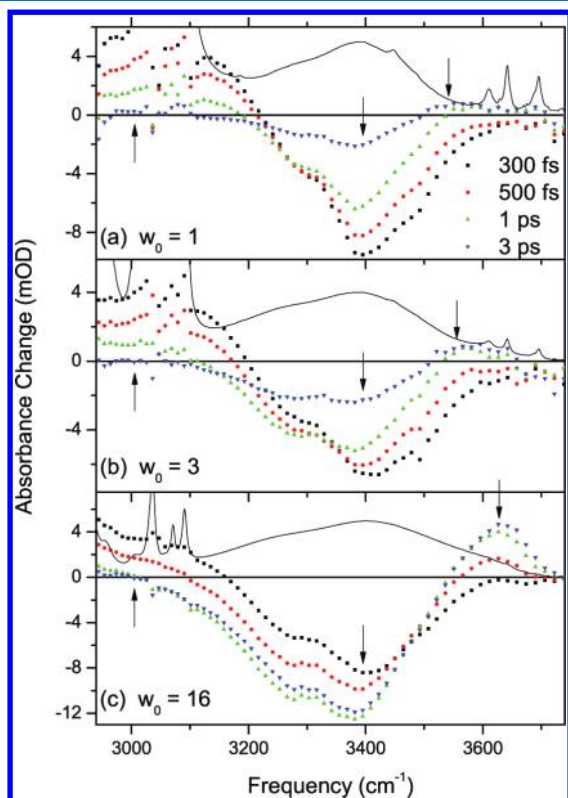


**Figure 2.** Transient pump–probe spectra after OH stretch excitation by pulses centered at  $3400\text{ cm}^{-1}$  for (a)  $w_0 = 1$ , (b)  $w_0 = 3$ , and (c)  $w_0 = 16$  (parallel linear polarization of pump and probe). The change of absorbance is plotted as a function of probe frequency for different delay times. The nonlinear response of the solvent benzene was subtracted from the measured absorption change. Solid lines: linear infrared absorption spectra. The arrows indicate frequency positions for which time-resolved transients are shown in Figures 4 and 5.

with pump pulses centered at  $3400\text{ cm}^{-1}$  as well as the respective linear absorption spectra (solid lines) for  $w_0 = 1, 3$ , and  $16$ . The absorbance change  $\Delta A$  measured with parallel polarization of pump and probe pulses is plotted as a function of probe frequency for four different pump–probe delays. In the spectra, we subtracted the weak nonlinear response of the neat solvent benzene which was independently measured under the same experimental conditions. The enhanced absorption at low probe frequencies is due to the  $\nu = 1$  to  $2$  transitions of the excited OH stretch oscillators, whereas the absorption decrease at higher frequencies originates from the bleaching of the  $\nu = 0$  ground state and stimulated emission on the  $\nu = 1$  to  $0$  transition. With increasing  $w_0$ , the decay of the enhanced absorption becomes faster, giving evidence of a decrease of the  $\nu = 1$  lifetime.

The line shape of the absorption decrease undergoes pronounced changes within the first 2 ps. For  $w_0 = 1$  and  $3$ , the center of the transient spectrum undergoes a shift to smaller frequencies, i.e., a red-shift, while its amplitude decreases for longer delay times. At late delays, a weak enhanced absorption builds up on the blue edge of the transient spectra. For  $w_0 = 16$ , the amplitude of the absorption decrease becomes larger

between 300 fs and 3 ps, and the bleaching broadens toward low frequencies. Concomitantly, a strong enhanced absorption builds up at the blue edge.

To quantify the spectral shifts of the absorption decrease, we calculated the time-dependent position of the first moment of the spectra (FM) given by

$$\text{FM} = \frac{\int \nu_{\text{Probe}} \Delta A(\nu_{\text{Probe}}) d\nu_{\text{Probe}}}{\int \Delta A(\nu_{\text{Probe}}) d\nu_{\text{Probe}}}$$

where  $\nu_{\text{Probe}}$  represents the probe frequency. To avoid contributions from the enhanced absorption features at low probe frequencies, the integration interval was limited to a frequency range of  $3193\text{--}3630\text{ cm}^{-1}$  for  $w_0 = 1$  and  $3$ . The lower limit represents the spectral position where the absorption decrease turns into the enhanced  $\nu = 1$  to  $2$  absorption. The upper limit was chosen to be as high as possible before more noisy features in the spectrum appear (due to lower probe intensity at these positions). With this approach, the enhanced absorption at later times also contributes. For  $w_0 = 16$ , the reshaping of the transient bands is stronger, requiring a variable lower frequency boundary which is determined by the  $\Delta A = 0$  position at the respective delay time.

In Figure 3, we show the time evolution of the FM. There is a pronounced acceleration of the spectral red-shift with

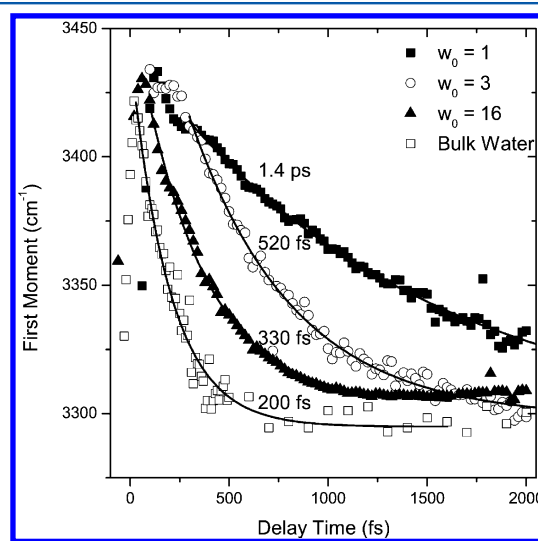


**Figure 3.** First moment (FM) of the transient spectra in Figure 2. The FM frequency (symbols) is plotted as a function of delay time for  $w_0 = 1, 3$ , and  $16$  and for bulk  $\text{H}_2\text{O}$ .<sup>28</sup> The solid lines represent single-exponential fitting curves with the time constants indicated. The FM kinetics speed up with increasing water concentration.

increasing hydration. Fitting a single-exponential kinetics to the time evolution of the FM gives the time constants indicated in Figure 3. We limit such analysis to delay times longer than 250 fs. At shorter delay times, pump and probe pulses overlap in time and, consequently, the sequential pump–probe signals are superimposed by third-order signals from the coherent pump–probe coupling. For  $w_0 = 16$ , a substantial part of the FM shift occurs within the first 250 fs. For comparison, we present the FM shift for OH stretch excitations in bulk water as derived from the data set published in ref 28.

**Time-Resolved Absorption Changes.** The kinetics of pump–probe signals were measured at different fixed probe



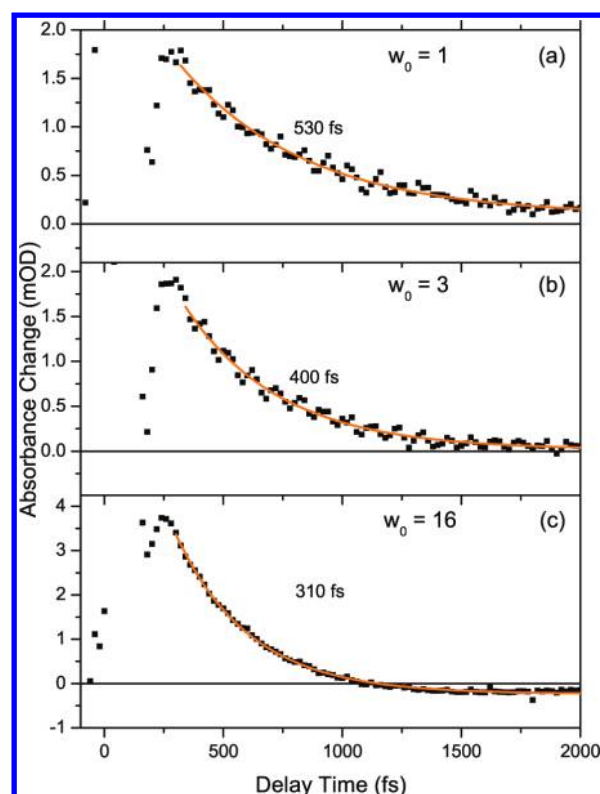


**Figure 4.** Time evolution of the transient  $\nu = 1$  to 2 absorption of excited OH stretching oscillators. The absorbance change measured at a probe frequency of  $3005\text{ cm}^{-1}$  with parallel linear polarizations of pump and probe pulses is plotted as a function of delay time for  $w_0 = 1, 3$ , and 16 (symbols). The solid lines are single-exponential fitting curves with the decay times indicated.

frequencies (arrows in Figure 2) to separate the different processes contributing to the time evolution of the transient spectra. In Figure 4, the time dependence of the enhanced absorption on the  $\nu = 1$  to 2 transition of the excited OH stretch oscillators is plotted for a probe frequency of  $3005\text{ cm}^{-1}$  (parallel linear polarization of pump and probe pulses). With increasing hydration level, the decay of  $\nu = 1$  to 2 absorption accelerates, reflecting a decrease of the  $\nu = 1$  lifetime from 530 fs at  $w_0 = 1$  to  $\sim 300$  fs at  $w_0 = 16$ . It should be noted that the  $\nu = 1$  lifetime of OH stretch excitations in bulk  $\text{H}_2\text{O}$  has a value of 200 fs.<sup>22</sup>

Normalized transients measured at a probe frequency of  $3395\text{ cm}^{-1}$ , i.e., close to the initial maximum of the absorption decrease in the transient spectra of Figure 2, are shown in Figure 5a. For  $w_0 = 1$  and 3, we present data measured with parallel linear polarization of pump and probe (symbols) as well as the respective rotation-free signals (solid lines). Such two sets of transients agree within the experimental accuracy, pointing to minor contributions of molecular reorientation and/or resonant energy transfer processes in the time range between 300 fs and a couple of picoseconds. Correspondingly, the pump–probe anisotropies derived from the absorption changes in this time interval have a constant value of  $r(t) \approx 0.25 \pm 0.1$  for  $w_0 = 1$  and  $r(t) \approx 0.15 \pm 0.1$  for  $w_0 = 3$ . For  $w_0 = 1$  and 3, the absorption decrease reaches its maximum amplitude at early delay times and then decays monotonically. In contrast, the  $w_0 = 16$  transient (measured with parallel linear polarizations) shows a narrow spike at early delay times, followed by a delayed rise up to 1.5 ps and a subsequent slow

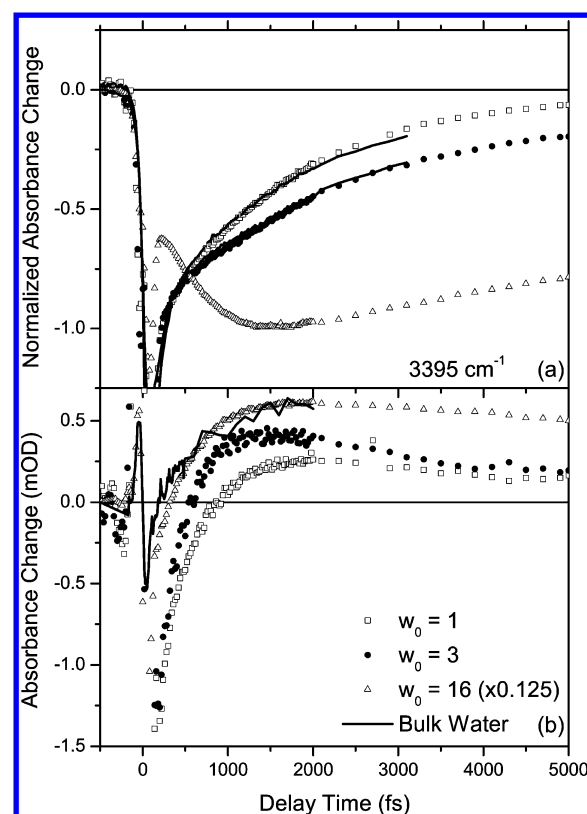


**Figure 5.** (a) Time evolution of the maximum bleach signal at  $3395\text{ cm}^{-1}$  for  $w_0 = 1, 3$ , and 16. Both data recorded with parallel linear polarizations of pump and probe pulses (symbols) and isotropic signals for  $w_0 = 1$  and  $w_0 = 3$  (lines) are shown. (b) Buildup kinetics of enhanced absorption at the blue edge of the OH stretching band. The micelle transients (symbols) were measured at the following spectral positions:  $3535\text{ cm}^{-1}$  ( $w_0 = 1$ ),  $3550\text{ cm}^{-1}$  ( $w_0 = 3$ ), and  $3625\text{ cm}^{-1}$  ( $w_0 = 16$ ) as indicated by the arrows in Figure 2. The absolute values of the absorption change for  $w_0 = 16$  were scaled with a factor of 0.125. For comparison, a transient for bulk water is shown (solid line, frequency position  $3580\text{ cm}^{-1}$ , scaled to the  $w_0 = 16$  transient). All transients were measured with parallel linear polarizations of pump and probe pulses.

decay. Here, the pump–probe anisotropy  $r(t)$  decays to zero within the first 300 fs. As coherent pump–probe coupling makes a strong contribution to the signal at such early times, we did not analyze the time evolution of  $r(t)$  in detail. The fact that none of the transients shown in Figure 5a match the enhanced absorption decays of Figure 3 demonstrates that—in addition to the  $\nu = 1$  population decay—other processes contribute to the transient behavior.

In Figure 5b, we present the time-dependent absorption increase at high probe frequencies (taken at the maximum of the blue-shifted enhanced absorption, cf. Figure 2). To facilitate a comparison of data taken with different  $w_0$ , we have rescaled the  $w_0 = 16$  transient by multiplying the measured change of absorbance with a factor of 0.125. For all  $w_0$  values, the time-dependent absorption enhancement displays a delay which is most pronounced for  $w_0 = 1$  and decreases for the higher values of  $w_0$ . For  $w_0 = 16$ , the position of the maximum around 1.5 ps agrees with that of the delayed minimum in the  $w_0 = 16$  transient of Figure 5a. After reaching the maximum, the signals slowly decay. Such decay is faster for lower water content. For comparison, we show a transient measured with a bulk water

sample and normalized to the amplitude of the  $w_0 = 16$  data (solid line, taken from the data set in ref 28).

In addition to the pump–probe measurements in the range of the OH stretch absorption, we studied the OH bending response after OH stretch excitation in two-color experiments. The inset of Figure 6 shows the transient OH bending spectra

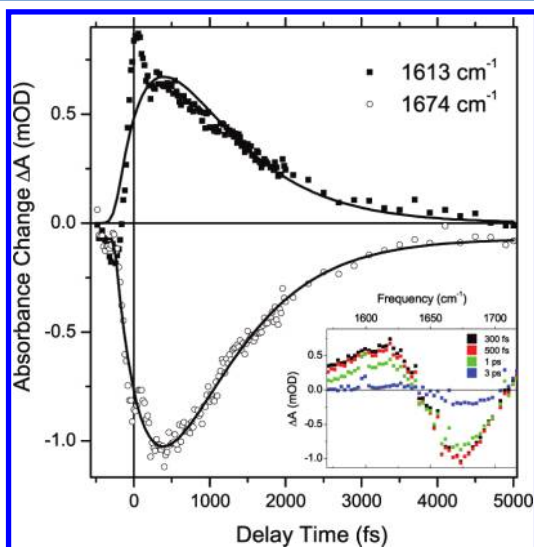


**Figure 6.** Time-resolved absorption changes in the range of the OH bending mode after OH stretch excitation of DOPC reverse micelles with  $w_0 = 1$ . The data show an enhanced absorption at a probe frequency of  $1613\text{ cm}^{-1}$  and an absorption decrease at  $1674\text{ cm}^{-1}$ . The solid lines represent kinetics calculated from a rate equation model with a 500 fs rise time which corresponds to the  $\nu = 1$  lifetime of the initially excited OH stretch oscillators and a 800 fs decay, representing the  $\nu = 1$  lifetime of the OH bending oscillator. All data were recorded with parallel linear polarization of pump and probe pulses. Inset: transient OH bending spectra for different pump–probe delays.

for  $w_0 = 1$  with an absorption decrease on the fundamental transition around  $1675\text{ cm}^{-1}$  and a red-shifted absorption increase due to the  $\nu = 1$  to 2 transition. The transients in Figure 6 display a sharp peak around delay zero which is due to coherent pump–probe coupling and superimposed on a delayed rise of the sequential pump–probe signals reaching their maxima around 500 fs. For comparison, double-exponential fits convoluted with the 150 fs time resolution of our experiment are shown as solid lines. The data fit well to a 500 fs rise time and subsequent 800 fs decay. The delayed rise nicely matches the 530 fs decay of the  $\nu = 1$  to 2 absorption of the excited OH stretch oscillators. It is important to note that the maxima in the OH bend transients occur at an earlier delay time than those of the blue-shifted enhanced absorption in the OH stretching range (Figures 2 and 5).

## DISCUSSION

Our experimental results give insight into the ultrafast spectral evolution of OH stretch excitations and into OH stretch relaxation and its pathways. Such processes are characterized by different ultrafast kinetics that change over the hydration ( $w_0$ ) range studied here. In the following, we first discuss the transient line shapes, followed by an analysis of the OH stretch relaxation scenario and the concomitant redistribution of vibrational excess energy.

**Transient Line Shapes of OH Stretch Absorption.** The transient spectra in Figure 2 and the time evolution of the FM

in Figure 3 demonstrate a pronounced reshaping of the transient OH stretching bands on a time scale depending on the respective hydration level. At  $w_0 = 1$ , the concentrations of DOPC and water molecules have a similar value of 0.25 M. As a result, individual water and DOPC molecules are interacting with each other, whereas the interaction between different water molecules is much weaker than in bulk water. Nevertheless, the linear OH stretching band (Figure 1) shows a substantial spectral width that points to a distribution of OH stretch frequencies for different water sites, i.e., structural inhomogeneity. Moreover, spectral diffusion of OH stretching excitations may contribute.

The spectral kinetics of the  $w_0 = 1$  FM plotted in Figure 3 (solid squares) show a fast initial shift to smaller frequency. The amplitude of this contribution is affected by the limited time resolution of the experiment and, moreover, may be distorted by the superposition of the coherent pump–probe coupling that contributes up to delay times of 250 fs. Nevertheless, one expects a transient red-shift caused by an ultrafast energy transfer from the antisymmetric to the symmetric OH stretching mode which is red-shifted by  $90\text{ cm}^{-1}$ . While the concept of antisymmetric and symmetric OH stretch modes is strictly valid for water monomers in the gas phase only, ultrafast time-resolved studies of water monomers in acetonitrile<sup>29</sup> have shown a fast decrease of the pump–probe anisotropy occurring on a 200 fs time scale, which points to intramolecular energy transfer between the two stretching modes. The similarity of the experimental conditions of ref 29, in particular the water concentration  $c \approx 0.3\text{ M}$ , with conditions we use for small  $w_0$  suggests the appropriateness of this description for isolated water molecules interacting with a phospholipid headgroup. In line with this interpretation, we find a value of the pump–probe anisotropy  $r(t) = 0.25 \pm 0.1$  for delay times longer than 250 fs, in the same range as the theoretical value of 0.1 one expects for a randomization between identical numbers of symmetric and antisymmetric water stretch transition dipoles of perpendicular orientation.<sup>30</sup> It should be noted that this fast energy transfer occurs well within the  $\nu = 1$  lifetime of the OH stretch oscillators of 530 fs (cf. Figure 4a).

After the initial fast shift of the FM, the  $w_0 = 1$  data in Figure 3 display a red-shift over a frequency interval of the order of  $100\text{ cm}^{-1}$  which roughly follows a single-exponential kinetics with a time constant of 1.4 ps. In principle, the 530 fs decay of the  $\nu = 1$  to 2 absorption at low frequencies (cf. Figure 4a), the delayed buildup of a weak blue-shifted absorption which overlaps with the original absorption band (cf. Figure 5b), and spectral diffusion of the OH stretch excitations contribute to a transient red-shift. It is important to note that (i) the 1.4 ps FM kinetics is much slower than the 530 fs population decay of the  $\nu = 1$  state and (ii) the frequency interval over which we integrated to determine the FM excludes the major part of the transient  $\nu = 1$  to 2 absorption. Thus, the  $\nu = 1$  decay makes a minor contribution to the observed FM red-shift. In contrast, the buildup of the blue-shifted absorption (Figure 5b) covers the same time range as the FM red-shift and compensates part of the negative absorption changes occurring at high probe frequencies. As a result, the picosecond kinetics of the FM shift reflect this compensation effect and a potential contribution of spectral diffusion. As pump–probe data do not allow for a reliable separation of the line shapes of the transient absorption decrease and of the blue-shifted absorption band, the exact time scale of spectral diffusion cannot be extracted from the overall FM shift. However, the time constant of 1.4 ps represents a

lower limit of the spectral diffusion time. This conclusion is supported by two-dimensional OH stretch spectra we will present elsewhere.

We attribute the drastic slowing down of spectral diffusion compared to bulk water mainly to the absence of a rapidly fluctuating force a water pool would exert on the OH stretch oscillators and to the minor role of direct water–water interactions and resonant OH stretch energy transfer.<sup>28</sup> Fluctuating Coulomb forces originating from the ionic groups of the DOPC molecules occur at low frequencies due to the comparably slow motions of the heavy ionic  $\text{PO}_4^-$  and choline groups. Another mechanism which may contribute to spectral diffusion on a slower time scale are fluctuations of hydrogen bond geometries between the individual water and DOPC molecules which may include the breaking and re-formation of hydrogen bonds. Such structural fluctuations have been invoked to explain a 1 ps decay component in the decay of frequency time correlation function of OD stretch excitations in small AOT reverse micelles filled with HOD/ $\text{H}_2\text{O}$ .<sup>14</sup>

The OH stretch FM shift becomes faster with increasing hydration level. The  $w_0 = 16$  data in Figure 3 (solid triangles) give evidence of a strongly accelerated spectral shift within the first 500 fs after excitation. Such kinetics are, however, still somewhat slower than the FM shift in bulk water (open squares in Figure 3) which is governed by spectral diffusion within the first 200 fs as observed in two-dimensional OH stretch spectra.<sup>28</sup> In both the  $w_0 = 16$  reverse micelles and bulk water, fluctuating forces originating from structural fluctuations of the hydrogen-bonded network of dipolar water molecules represent a major source of spectral diffusion. In addition, resonant vibrational energy transfer between OH stretching oscillators comes into play. It has been shown for bulk water that both mechanisms contribute to the observed fast spectral diffusion and to a concomitant decay of the pump–probe anisotropies.<sup>28,31</sup> Water in the  $w_0 = 16$  reverse micelles displays pronounced structural inhomogeneity arising from water molecules at the DOPC surface, which show slower structural dynamics and energy transfer, along with water molecules in the reverse micellar core, which undergo faster, bulklike fluctuations and energy transfer. The FM shift is a quantity averaged over the whole ensemble, and the average FM kinetics are, thus, slower than in bulk water.

For  $w_0 = 16$ , the FM shifts measured at delay times longer than 300–400 fs are governed by the buildup of a vibrationally hot ground state of the water pool (see below) which affects the OH stretch line shape in a very broad range.<sup>32,33</sup> A hallmark of this mechanism is the rise of the bleaching amplitudes at delay times between 300 fs and 3 ps (Figure 5a) and the formation of the strong blue-shifted absorption which peaks at  $3620\text{ cm}^{-1}$ .

**Vibrational Relaxation and Energy Dissipation.** The decay of the  $\nu = 1$  to 2 absorption gives the most direct information on the  $\nu = 1$  lifetime of the OH stretch oscillators. The data in Figure 3 clearly show that this lifetime decreases from 530 fs at  $w_0 = 1$  to  $\sim 300$  fs at  $w_0 = 16$ . While a similar behavior has been observed for water in AOT reverse micelles, its origin and underlying relaxation pathways have remained controversial. Recent studies of water molecules bound to different surfactants like AOT in reverse micelles<sup>16,18</sup> and phospholipids in lipid bilayers<sup>23</sup> have been interpreted in terms of a predominant relaxation into low-frequency hydrogen bond and solvent modes. On the other hand, OH stretch excitations of bulk water relax via the OH bending mode.<sup>22,33</sup>

The results presented in Figure 6 clearly show that OH stretching excitation at  $w_0 = 1$  induces a transient change of OH bending absorption. The OH bend absorption changes consist of a bleaching on the fundamental ( $\nu = 0$  to 1) transition and a red-shifted enhanced absorption, both building up with a rise time of  $\sim 500$  fs. This rise time is very close to the  $\nu = 1$  lifetime of the initially excited OH stretch oscillators but substantially faster than the buildup of enhanced absorption at high OH stretching frequencies (cf. Figure 5), the latter being caused by a vibrationally hot ground state (see below). We, thus, attribute the changes of OH bending absorption after OH stretch excitation to a population transfer from the excited OH stretch oscillator to the OH bend oscillator of the same molecule. In this process which represents the predominant OH stretch relaxation channel, a transient population of the  $\nu = 1$  state of the OH bend oscillator is generated with a rise time identical to the lifetime of the  $\nu = 1$  OH stretch state. The transient population of the  $\nu = 1$  state of the OH bend oscillator causes the bleaching of the OH bend fundamental and an enhanced red-shifted absorption on the  $\nu = 1$  to 2 transition. This mechanism involves a nonadiabatic coupling between the  $\nu = 1$  state of the OH stretching mode and the  $\nu = 2$  overtone of the bending mode. From the frequency positions of bleaching and enhanced absorption in the transient OH bend spectra (inset of Figure 6a), one estimates a frequency position of the OH bend overtone level at  $\nu = 1675 + 1625\text{ cm}^{-1} = 3300\text{ cm}^{-1}$ . This position agrees well with the shoulder in the linear OH stretch absorption spectra (Figure 1) and is in the range of the  $\nu = 1$  state of the OH stretch oscillators. In this relaxation scenario, the lifetime of the OH stretching mode in  $\nu = 1$  depends upon the nonadiabatic coupling and energy mismatch between the  $\nu = 1$  OH stretch and the  $\nu = 2$  OH bend states. With increasing hydration level, spectral diffusion leads to increasing fluctuations in the positions of such two levels which is expected to accelerate OH stretch relaxation by transiently reducing their energy mismatch. The observed shortening of the OH stretch lifetime with increasing  $w_0$  is fully in line with this picture.

The OH bend vibration is the lowest intramolecular mode of  $\text{H}_2\text{O}$ , and thus, its population relaxation requires a coupling to modes of the environment. After OH stretch excitation, such coupling to the environment is relevant for the relaxation from the  $\nu = 2$  to the  $\nu = 1$  state of the OH bend oscillator and for the subsequent decay of the  $\nu = 1$  state. In bulk water with an OH stretch lifetime of 200 fs and an OH bend lifetime of 170 fs,<sup>22</sup> OH bend relaxation involves librational motions of the OH bend-excited water molecule and a fast energy dissipation through other intermolecular librational modes of the environment.<sup>33,34</sup> In bulk water, the changes of OH bend absorption after OH stretch excitation display different kinetics of the  $\nu = 1$  to 2 enhanced absorption and the  $\nu = 0$  to 1 absorption decrease, the latter being strongly influenced by the energy dissipation to the environment.<sup>22</sup> In contrast, the data in Figure 6 display similar kinetics of the enhanced absorption around  $1625\text{ cm}^{-1}$  and the absorption decrease around  $1675\text{ cm}^{-1}$ , both showing the delayed rise and a subsequent decay with a time constant of the order of 1 ps, the lifetime of the  $\nu = 1$  state of the OH bend oscillator. This picosecond lifetime, which is much longer than in bulk water, points to a markedly different local environment of the excited water molecules in which librational motions may be shifted in frequency or even hindered by the interaction with the DOPC molecule nearby and, thus, other relaxation channels, e.g., those involving DOPC modes, may come into play. In any case, the manifold of



intermolecular water librations is absent because of the low water concentration of  $c \approx 0.25$  M.

The vibrational excess energy released in the decay of the OH stretch and bend modes of excited water molecules is randomized via low-frequency excitations of the system to create a vibrationally hot ground state.<sup>32,33</sup> At a low hydration level ( $w_0 = 1$ ), the DOPC molecules and, subsequently, the solvent benzene serve as acceptors of excess energy. At a high hydration level ( $w_0 = 16$ ), the pool of water molecules represents the primary heat sink from which excess energy is transferred to the DOPC and eventually to the benzene solvent on a slower time scale. At  $w_0 = 16$ , the spectral signatures of the hot water ground state are the blue-shifted transient OH stretch absorption at frequencies around  $3600\text{ cm}^{-1}$  and the enhanced absorption decrease over nearly the entire OH stretching band (Figure 2c). The blue-shifted OH stretch absorption is due to water molecules with weakened and/or broken hydrogen bonds. For  $w_0 = 16$ , this absorption builds up on a subpicosecond time scale and reaches a maximum after 1.5 ps (Figure 5 b). Such kinetics are very close to bulk water (solid line in Figure 5b).<sup>28,33</sup> In contrast to bulk water, however, the enhanced absorption decays again on a time scale of tens of picoseconds due to an energy transfer from the heated water pool in the micelle to the surrounding solvent benzene.<sup>21</sup> It should be noted that in our previous study investigating dynamics of phosphate stretching excitations in DOPC reverse micelles, we observed the intramolecular water pool as the primary sink for excess vibrational energy.<sup>11</sup>

The transient spectra for smaller  $w_0$  values (Figure 2a,b) show a much weaker and less blue-shifted OH stretch absorption at long delay times and a slower buildup of this component (Figure 5b). Here, the DOPC molecules play a more prominent role in accepting excess energy. The weak blue-shifted absorption points to weaker local interactions between water and DOPC molecules, in particular at  $w_0 = 1$  where a water pool is absent. The slower buildup of enhanced absorption reflects the longer OH stretch and bend lifetimes at lower hydration levels (cf. Figures 4 and 6), resulting in a slower energy transfer into the DOPC vibrational manifold. Eventually, the excess energy flows into the benzene environment as is evident from the decay of the enhanced absorption in the picosecond time domain.

## CONCLUSIONS

In conclusion, we have studied OH stretching excitations of water in DOPC reverse micelles, a phospholipid model system, to map the structural dynamics of confined water and vibrational relaxation processes. The experiments cover a wide range of hydration levels from a 1:1 ratio of DOPC and water molecules up to a 16:1 ratio. At low water content, spectral diffusion within the first 300 fs is due to an energy transfer from the asymmetric to the symmetric OH stretching mode, followed by a much slower spectral shift which sets a lower limit of 1.4 ps for the spectral diffusion time. With increasing hydration level, spectral diffusion accelerates and the structural fluctuations of the water pool become the prominent factor driving spectral fluctuations. At low hydration, OH stretch excitations decay via the nonadiabatically coupled OH bending mode, similar to bulk water, as is evident from the measurement of transient OH bend populations after OH stretch excitation. Increasing spectral diffusion at higher hydration levels is effective in bridging the energy gap between the  $\nu = 1$  OH stretch and the  $\nu = 2$  OH bend states, resulting in

a shortening of the OH stretch lifetime. At high hydration levels, vibrational excess energy released in the OH stretch relaxation is initially randomized in the water pool, whereas DOPC molecules serve as the primary energy acceptor at low hydration. For a more detailed characterization of the different processes, two-dimensional infrared spectra of the different water excitations are required. Such work is presently underway.

## AUTHOR INFORMATION

### Corresponding Author

\*E-mail: costard@mbi-berlin.de (R.C.); elsasser@mbi-berlin.de (T.E.).

### Notes

The authors declare no competing financial interest.

## ACKNOWLEDGMENTS

This research has received funding from the European Research Council under the European Union's Seventh Framework Programme (FP7/2007-2013)/ERC grant agreement no. 247051.

## REFERENCES

- (1) Chaplin, M. *Nat. Rev.* **2006**, *7*, 861–866.
- (2) Ball, P. *Chem. Rev.* **2008**, *108*, 74–108.
- (3) Nibbering, E. T. J.; Elsaesser, T. *Chem. Rev.* **2004**, *104*, 1887–1914.
- (4) Bakker, H. J.; Skinner, J. L. *Chem. Rev.* **2010**, *110*, 1498–1517.
- (5) Volkov, V. V.; Palmer, D. J.; Righini, R. *Phys. Rev. Lett.* **2007**, *99*, 078302.
- (6) Zhao, W.; Moilanen, D. E.; Fenn, E. E.; Fayer, M. D. *J. Am. Chem. Soc.* **2008**, *130*, 13927–13937.
- (7) Szyc, L.; Yang, M.; Elsaesser, T. *J. Phys. Chem. B* **2010**, *114*, 7951–7957.
- (8) Yang, M.; Szyc, L.; Elsaesser, T. *J. Phys. Chem. B* **2011**, *115*, 13093–13100.
- (9) Luisi, P. L.; Giomini, M.; Pileni, M. P.; Robinson, B. H. *Biochim. Biophys. Acta* **1988**, *947*, 209–246.
- (10) De, T. K.; Maitra, A. *Adv. Colloid Interface Sci.* **1995**, *59*, 95–193.
- (11) Levinger, N. E.; Costard, R.; Nibbering, E. T. J.; Elsaesser, T. *J. Phys. Chem. A* **2011**, *115*, 11952–11959.
- (12) Faeder, J.; Ladanyi, B. M. *J. Phys. Chem. B* **2000**, *104*, 1033–1046.
- (13) Piletic, I. R.; Moilanen, D. E.; Spry, D. B.; Levinger, N. E.; Fayer, M. D. *J. Phys. Chem. A* **2006**, *110*, 4985–4999.
- (14) Fenn, E. E.; Wong, D. B.; Giammanco, C. H.; Fayer, M. D. *J. Phys. Chem. B* **2011**, *115*, 11658–11670.
- (15) Dokter, A. M.; Woutersen, S.; Bakker, H. J. *Proc. Natl. Acad. Sci. U. S. A.* **2006**, *103*, 15355–15358.
- (16) Dokter, A. M.; Woutersen, S.; Bakker, H. J. *Phys. Rev. Lett.* **2005**, *94*, 178301.
- (17) Cringus, D.; Lindner, J.; Milder, M. T. W.; Pshenichnikov, M. S.; Vöhringer, P.; Wiersma, D. A. *Chem. Phys. Lett.* **2005**, *408*, 162–168.
- (18) Cringus, D.; Bakulin, A.; Lindner, J.; Vöhringer, P.; Pshenichnikov, M. S.; Wiersma, D. A. *J. Phys. Chem. B* **2007**, *111*, 14193–14207.
- (19) Pieniazek, P. A.; Lin, Y. S.; Chowdhary, J.; Ladanyi, B. M.; Skinner, J. L. *J. Phys. Chem. B* **2009**, *113*, 15017–15028.
- (20) Seifert, G.; Patzlaff, T.; Graener, H. *Phys. Rev. Lett.* **2002**, *88*, 147402.
- (21) Deak, J. C.; Pang, Y.; Sechler, T. D.; Wang, Z.; Dlott, D. D. *Science* **2004**, *306*, 473–476.
- (22) Ashihara, S.; Huse, N.; Espagne, A.; Nibbering, E. T. J.; Elsaesser, T. *Chem. Phys. Lett.* **2006**, *424*, 66–70.

- (23) Ghosh, A.; Smits, M.; Bredenbeck, J.; Bonn, M. *J. Am. Chem. Soc.* **2007**, *129*, 9608–9609.
- (24) Foglia, F.; Lawrence, M. J.; Lorenz, C. D.; McLain, S. E. *J. Chem. Phys.* **2010**, *133*, 145103.
- (25) Pettitt, B. M.; Rossky, P. J. *J. Chem. Phys.* **1986**, *84*, 5836–5844.
- (26) Laage, D.; Stirnemann, G.; Sterpone, F.; Rey, R.; Hynes, J. T. *Annu. Rev. Phys. Chem.* **2011**, *62*, 395–416.
- (27) Kaindl, R. A.; Wurm, M.; Reimann, K.; Hamm, P.; Weiner, A. M.; Woerner, M. *J. Opt. Soc. Am. B* **2000**, *17*, 2086–2094.
- (28) Kraemer, D.; Cowan, M. L.; Paarmann, A.; Huse, N.; Nibbering, E. T. J.; Elsaesser, T.; Miller, R. J. D. *Proc. Natl. Acad. Sci. U. S. A.* **2008**, *105*, 437–442.
- (29) Cringus, D.; Jansen, T. I. C.; Pshenichnikov, M. S.; Wiersma, D. *A. J. Chem. Phys.* **2007**, *127*, 084507.
- (30) Fleming, G. R. *Chemical Applications of Ultrafast Spectroscopy*; Oxford University Press: New York, 1986.
- (31) Jansen, T. L. C.; Auer, B. M.; Yang, M.; Skinner, J. L. *J. Chem. Phys.* **2010**, *132*, 224503.
- (32) Lock, A. J.; Bakker, H. J. *J. Chem. Phys.* **2002**, *117*, 1708–1722.
- (33) Ashihara, S.; Huse, N.; Espagne, A.; Nibbering, E. T. J.; Elsaesser, T. *J. Phys. Chem. A* **2007**, *111*, 743–746.
- (34) Rey, R.; Ingrosso, F.; Elsaesser, T.; Hynes, J. T. *J. Phys. Chem. A* **2009**, *113*, 8949–8962.